PERVASIVE FAINT Fe XIX EMISSION FROM A SOLAR ACTIVE REGION OBSERVED WITH EUNIS-13: EVIDENCE FOR NANOFLARE HEATING

Jeffrey W. Brosius[1], Adrian N. Daw[2], and D. M. Rabin[3]

[1] Catholic University of America at NASA Goddard Space Flight Center, Solar Physics Laboratory, Code 671,
Greenbelt, MD 20771, USA; Jeffrey.W.Brosius@nasa.gov
[2] NASA Goddard Space Flight Center, Solar Physics Laboratory, Code 671, Greenbelt, MD 20771, USA
[3] NASA Goddard Space Flight Center, Heliophysics Science Division, Code 670, Greenbelt, MD 20771, USA
Received 2014 March 16; accepted 2014 June 12; published 2014 July 10

ABSTRACT

We present spatially resolved EUV spectroscopic measurements of pervasive, faint Fe XIX 592.2 Å line emission in an active region observed during the 2013 April 23 flight of the Extreme Ultraviolet Normal Incidence Spectrograph (EUNIS-13) sounding rocket instrument. With cooled detectors, high sensitivity, and high spectral resolution, EUNIS-13 resolves the lines of Fe XIX at 592.2 Å (formed at temperature $T \approx 8.9$ MK) and Fe XII at 592.6 Å ($T \approx 1.6$ MK). The Fe XIX line emission, observed over an area in excess of 4920 arcsec^2 (2.58×10^9 km^2, more than 60% of the active region), provides strong evidence for the nanoflare heating model of the solar corona. No *GOES* events occurred in the region less than 2 hr before the rocket flight, but a microflare was observed north and east of the region with *RHESSI* and EUNIS during the flight. The absence of significant upward velocities anywhere in the region, particularly the microflare, indicates that the pervasive Fe XIX emission is not propelled outward from the microflare site, but is most likely attributed to localized heating (not necessarily due to reconnection) consistent with the nanoflare heating model of the solar corona. Assuming ionization equilibrium we estimate Fe XIX/Fe XII emission measure ratios of ∼0.076 just outside the AR core and ∼0.59 in the core.

Key words: Sun: activity – Sun: corona – Sun: flares – Sun: UV radiation

1. INTRODUCTION

Although it has been more than 70 yr since Grotrian (1939) and Edlén (1943) demonstrated that the solar corona is comprised of million-degree plasma, a widely accepted explanation for this counterintuitive phenomenon remains elusive. A number of coronal heating mechanisms have been proposed, including, for example, dissipation of Alfvén waves (Alfvén 1947; Ionson 1978; Hollweg 1984; Davila 1987; van Ballegooijen et al. 2011; McIntosh et al. 2011), chromospheric jets or type II spicules (De Pontieu et al. 2009, 2011; Judge et al. 2012), and nanoflares (Glencross 1975; Parker 1983, 1988; Lin et al. 1984; Cargill 1994; Klimchuk 2009).

The nanoflare heating model has recently attracted considerable attention because of improved theoretical calculations and new observations (Klimchuk et al. 2008; Bradshaw & Klimchuk 2011; Viall & Klimchuk 2011, 2012, 2013; Warren et al. 2011; Mulu-Moore et al. 2011; Bradshaw et al. 2012; Reep et al. 2013). This scenario envisions the ubiquitous presence of tiny, independent heating events (likely but not necessarily due to magnetic reconnection) occurring on individual sub-resolution strands within coronal loops. Each of these heating events raises the strand plasma to temperatures ∼6–10 MK, much greater than the average active region temperature of ∼2 MK. After the impulsive energy release, the loop strand cools by conduction (which can drive chromospheric evaporation) and radiation. The temperature reached by the heated plasma depends on the amount of energy released in the nanoflare event. A plethora of such heating and cooling events, none individually detectable, produces the observed "average" corona. In addition, very faint emission at flare-like temperatures is expected to be present at all times, independent of ordinary flares. Observations of this emission would provide confirmation of the nanoflare heating model (Cargill 1994, 2013; Klimchuk 2009; Patsourakos & Klimchuk 2009; Bradshaw & Klimchuk 2011).

Reale et al. (2009b) and Schmelz et al. (2009b) report evidence of small amounts of plasma with temperatures up to 10 MK in active regions based on observations with *Hinode*'s X-Ray Telescope (XRT) alone, while Reale et al. (2009a) and Schmelz et al. (2009a) report further evidence based on coordinated observations with XRT and the *Ramaty High Energy Solar Spectroscopic Imager* (*RHESSI*). Here "small amounts" means that the emission measure of the high temperature plasma is about 2 orders of magnitude less than the emission measure of the typical coronal plasma around 2 MK. Testa et al. (2011) report evidence based on coordinated observations with *Hinode*'s XRT and Extreme-ultraviolet Imaging Spectrometer (EIS). In all cases, however, instrumental limitations precluded a definitive detection. Indeed, Winebarger et al. (2012) demonstrated that the combination of XRT and EIS is unable to provide accurate determinations of the presence of small amounts of hot plasma in the 6–10 MK temperature range, making it very difficult to detect the presence of nanoflare-heated plasma. Sylwester et al. (2010) used the RESIK X-ray spectrometer on the Russian *CORONAS-F* satellite to find similarly small amounts of high-temperature plasma in whole-Sun spectra during particularly quiet times; however, *GOES* A9-B5 events were always present, contributing to the high-temperature emission.

Viall & Klimchuk (2011) report that light curves of coronal loops and the diffuse corona observed with the *Solar Dynamics Observatory*'s Atmospheric Imaging Assembly (*SDO*/AIA; Lemen et al. 2012) EUV channels exhibit predictable and understandable patterns consistent with light curves derived from theoretical models of impulsive nanoflare heating in the cooling phase. However, such indirect evidence of nanoflare heating could not be confirmed by direct detection because the two (94 Å and 131 Å) channels centered on key flare lines likely to be produced by nanoflare-heated plasmas are dominated by emission from plasma at typical (1–3 MK) coronal

temperatures (Boerner et al. 2012; Brosius & Holman 2012). Rapid cadence (5.5 s) high spatial resolution (∼0″.1) narrow band 193 Å imagery from the Hi–C sounding rocket instrument (Cirtain et al. 2013) reveals variability on timescales of 15–20 s in areas of moss, which Testa et al. (2013) interpreted as coronal nanoflare heating events. In a different investigation of Hi-C images, Winebarger et al. (2013) studied rapidly evolving loop-like structures and concluded that they were cool (≈0.25 MK) and that their rapid temporal evolution was due to a combination of impulsive ("nanoflare") heating and rapid radiative cooling of the dense, low-lying plasma. Here, too, the evidence was indirect in the sense that Hi–C did not detect plasma at temperatures ∼10 MK.

Observations of individual spectral lines are essential to reveal the "smoking gun" of nanoflare heating. Spectroscopy is the only unambiguous way to resolve flare lines from nearby lines formed at ordinary coronal temperatures or cooler. Testa & Reale (2012) derived images of two active regions in Ca XVII 192.858 Å line emission (formed at temperatures ≈5.6 MK) observed with EIS to corroborate the presence of Fe XVIII (≈7.1 MK) emission in those same regions observed in AIA's 94 Å passband. The Ca XVII line at 192.858 Å is blended with two Fe XI lines and six O V lines. Ko et al. (2009) developed a procedure for extracting the Ca XVII contribution from the blend, but concluded that the procedure is unreliable when the intensity of the Ca XVII line itself is less than about 10% of the total intensity of the blend. Because the de-blending procedure is satisfactory only in areas where the Ca XVII line intensity is relatively strong, the method is not applicable for detecting weak nanoflare emission in typical areas of quiescent active regions with typical temperatures of 2–3 MK. This underscores the fact that a direct detection of the very hot plasma resulting from the nanoflare impulsive phase with AIA is extremely challenging.

To our knowledge, no evidence for the signature of nanoflare heating has been reported based on spectra from the *Solar and Heliospheric Observatory*'s Coronal Diagnostic Spectrometer (CDS), which observes the fairly bright Fe XIX line at 592.236 Å, formed at temperatures around 8.9 MK. This line has been observed during flares in CDS stare studies (e.g., Brosius 2003, Brosius & Phillips 2004, Brosius & Holman 2009) and raster studies (e.g., Czaykowska et al. 1999; Milligan et al. 2006; Teriaca et al. 2006), but is absent from the quiet Sun spectral atlas presented by Brooks et al. (1999). Here we present EUV spectroscopic measurements of faint emission in this Fe XIX line from an extensive portion of AR 11726 observed during the 2013 April 23 flight of the Extreme Ultraviolet Normal Incidence Spectrograph (EUNIS-13) sounding rocket instrument. We interpret this detection as strong evidence for the nanoflare heating scenario. In Section 2 we describe EUNIS-13, in Section 3 we present the observations and their analysis, in Section 4 we give the results of our analysis, in Section 5 we discuss and interpret our results, and in Section 6 we summarize our conclusions.

2. EUNIS-13

EUNIS is a two-channel imaging spectrograph that observes the Sun with high spectral resolution and a rapid cadence made possible by unprecedented sensitivity. The EUNIS flight at 17:30 UT on 2013 April 23 (EUNIS-13) included two major upgrades relative to the instrument's two previous flights (Brosius et al. 2007, 2008a, 2008b; Jess et al. 2008; Wang et al. 2010, 2011). First, the Active Pixel Sensor (APS) detectors were cooled to increase the dynamic range of recorded spectra

(by almost an order of magnitude) and reduce noise. Second, the grating in the 170–210 Å channel was replaced with an advanced Toroidal Varied Line Space (TVLS) grating so that we observed the 525–635 Å bandpass with the best dynamic range and 1st-order spectral resolution ever achieved by an imaging spectrometer at these wavelengths. Thus, EUNIS-13 observed in 300–370 and 525–635 Å wavebands, with spatial resolutions ∼4″ and 3″, respectively.

The 636″ EUNIS-13 slits were rotated about 3° clockwise from solar east–west. The EUNIS-13 observing sequence consisted of two main parts. In the first part, the pointing started near the center of AR 11726 (N13W49) and scanned ±45″ across the region by moving southward 45″, then northward 90″, southward 90″, northward 90″, and, finally, southward 45″ to return to its initial pointing position. Each full raster in this first part comprised 32 exposures and required almost 41 s to complete. The second part of the observing sequence involved similar but smaller rasters over AR 11723 at the southwest limb, and extended about two arcmin above the limb.

EUNIS-13 spectra were recorded in 690 pixels along the slit, each covering 0″.92, which over-samples the nominal 3″ spatial resolution by a factor of about 3. In order to reduce the noise and to bring the effective spatial resolution into closer agreement with the nominal resolution of the optical system, we averaged the EUNIS spectra over three consecutive spatial pixels. This, combined with the slit's pointing shift rate of 2″.14 s^{-1} perpendicular to the length of the slit (motion is directed nearly along the solar y-axis) during the 1.32 s exposures in AR 11726, yields a net pixel size of 2″.77 × 2″.82. In this work we focus primarily on the 32 exposures that comprise the first full northward-directed raster of AR 11726 (17:32:45–17:33:26 UT). The central time of this 41 s raster is 17:33:06 UT. The absolute radiometric calibration of the EUNIS-13 spectra is still preliminary.

As is typically the case with EUV spectrometers, EUNIS-13 does not incorporate an absolute wavelength scale. To obtain such a scale, we averaged the EUNIS-13 spectra over large areas (370″ × 90″) of quiet Sun within the 96 exposures that contain the first 3 complete scans across AR 11726. We performed profile fits (in spectral pixel units) to about 10 lines in each of the 3 APS units in the long wavelength channel to determine the centroids of each line, and equated those to the nominal rest wavelengths listed in the CHIANTI v.7.1 database (Dere et al. 1997; Landi et al. 2013). The wavelength scale was subsequently derived by cubic spline interpolation. There is, of course, no guarantee that all or any of the lines are at rest in the average quiet Sun spectrum, and subtle instrumental effects that produce wavelength drifts as a function of time cannot a priori be ruled out. In what follows, however, we are interested in wavelength *shifts* between one spatial area and another at nearly the same time, from which we derive relative (not absolute) Doppler velocities. Thus, for our purposes, the wavelength scale itself is not as important as are wavelength shifts between different areas for any given line.

3. OBSERVATIONS AND ANALYSIS

Our primary goal here is to report the unambiguous detection of faint emission from the ∼6–10 MK plasma that is theoretically predicted to be the best indicator of coronal heating by nanoflares (Cargill 1994, 2013; Klimchuk 2009; Patsourakos & Klimchuk 2009; Bradshaw & Klimchuk 2011). Toward this end, we focus on the Fe XIX line at 592.236 Å, formed at temperatures around 8.9 MK. To obtain the best possible profile
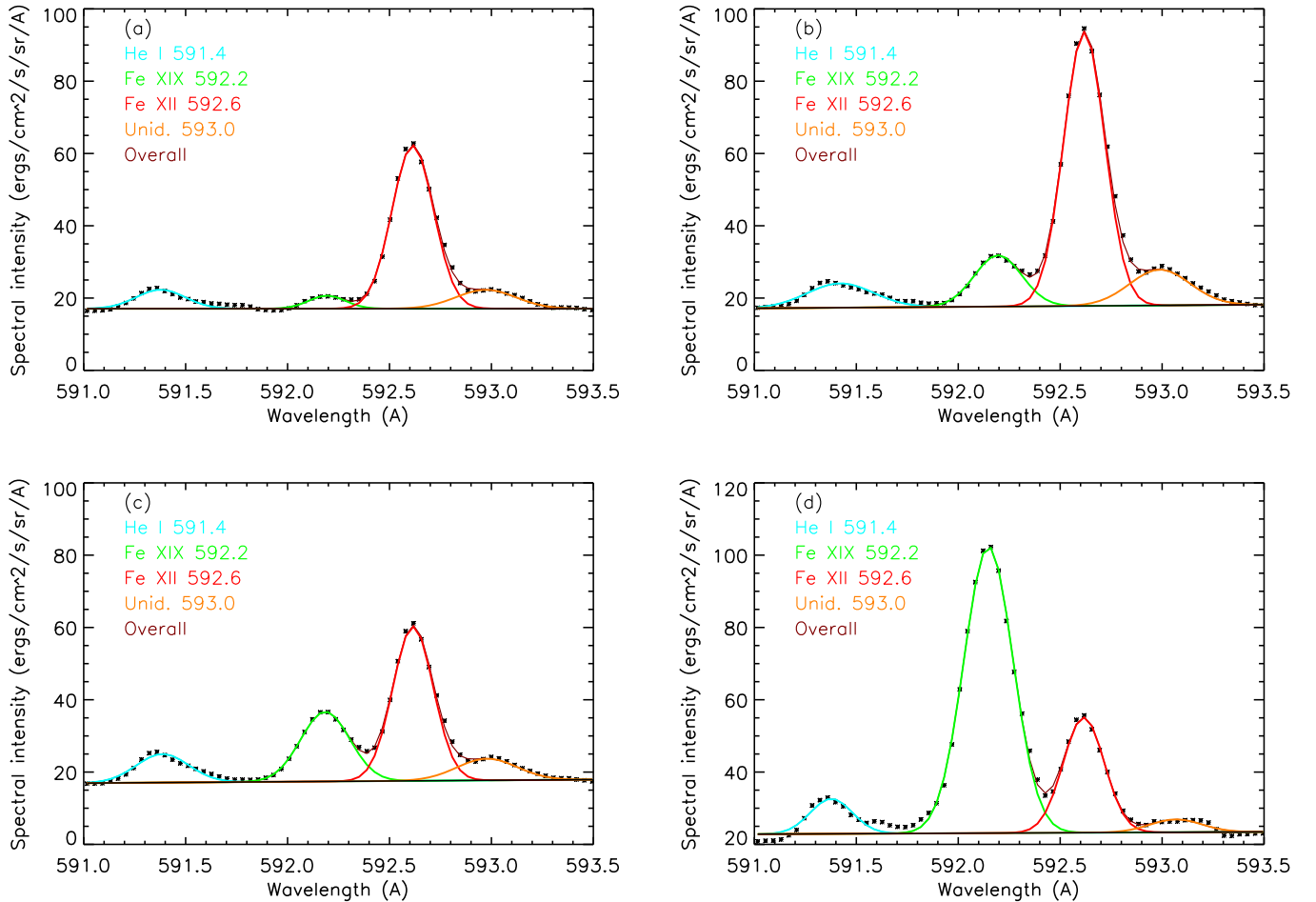
Figure 1. Line profile fits to Fe XIX and its neighbors in EUNIS-13 spectra obtained during the first full northward scan across AR 11726 averaged over four different intensity zones, all of which exclude the microflare. (a) shows the spectrum averaged over pixels in which the Fe XII 592.6 Å line intensity exceeds one-fourth (8.25 erg cm^{-2} s^{-1} sr^{-1}) its maximum value while the Fe XIX 592.2 Å line intensity remains less than 4 erg cm^{-2} s^{-1} sr^{-1}. (b) shows the spectrum averaged over pixels in which the Fe XII line intensity exceeds one-half (16.5) its maximum value. (c) shows the spectrum averaged over pixels in which the Fe XIX line intensity is between 4 and 16, while (d) shows the spectrum averaged over pixels in which the Fe XIX line intensity is between 16 and 64. All of the relevant contour levels are displayed in Figure 2. Fits to the various spectral components are color coded as indicated, where "overall" refers to the sum of the four Gaussian profiles and the spectral background. Integrated intensities of the Fe XIX and Fe XII lines are given in the text.

fit and the best value for the line's integrated intensity (using our preliminary absolute calibration), we select a wavelength range (591.0–593.5 Å) that is devoid of lines at each end (based on the CHIANTI line list, the CDS spectral catalog of Brooks et al. 1999, and EUNIS-13 spectra) so that our line profile fitting procedure is able to determine a reliable spectral background. Four lines are in this wavelength range, including: He I 591.412 Å, formed at temperature ($\approx$0.02 MK) characteristic of the upper chromosphere; Fe XIX 592.236 Å, formed at temperature ($\approx$8.9 MK) characteristic of flare plasma; Fe XII 592.601 Å, formed at temperature ($\approx$1.6 MK) characteristic of the quiescent active corona; and an unidentified line around 593 Å. The Fe XIX line was observed in only flare spectra by CDS. The Fe XII line was observed but not identified in the CDS quiet Sun spectral line catalog presented by Brooks et al. (1999) and in the SUMER off-limb quiescent spectral line catalog presented by Feldman et al. (1997); the line was identified by Del Zanna & Mason (2005) based on off-limb CDS spectra above QS areas. Feldman et al. (1997) also report the unidentified line at 593.08 Å, which they saw in second order, but they list no other lines that would blend with our EUNIS spectra between 591.0 and 593.5 Å.

Figure 1 shows Gaussian profile fits to spectra averaged over areas in which the integrated Fe XIX line intensity increases progressively from (a)–(d). These exemplify the variety encountered in the spatially resolved spectra whose profiles are fit to derive the integrated intensity images in Figure 2. All four lines are well resolved and color-coded as indicated. The spectral lines were fitted using the XCFIT and CFIT_BLOCK procedures developed for analysis of *SOHO*/CDS spectra in the SolarSoft IDL environment by Haugan (1997). These versatile procedures enable us to obtain each fitted profile's parameters (amplitude, centroid wavelength, and FWHM intensity), and provide two-dimensional maps of the results. Images of AR 11726 in Fe XIX 592.2 Å emission and Fe XII 592.6 Å emission are shown in Figure 2. This is the first time that a solar active region has been imaged in this Fe XII line.

The areas over which the spectra were averaged to obtain the profiles shown in Figure 1 were selected based on intensities displayed in Figures 2(a) and (b), as described in what follows. All the relevant intensity values are drawn as contours in Figure 2. In all cases we specifically excluded spectra within the microflare around (+595″, +295″) from those used to obtain the average profiles. Figure 1(a) shows the spectrum averaged
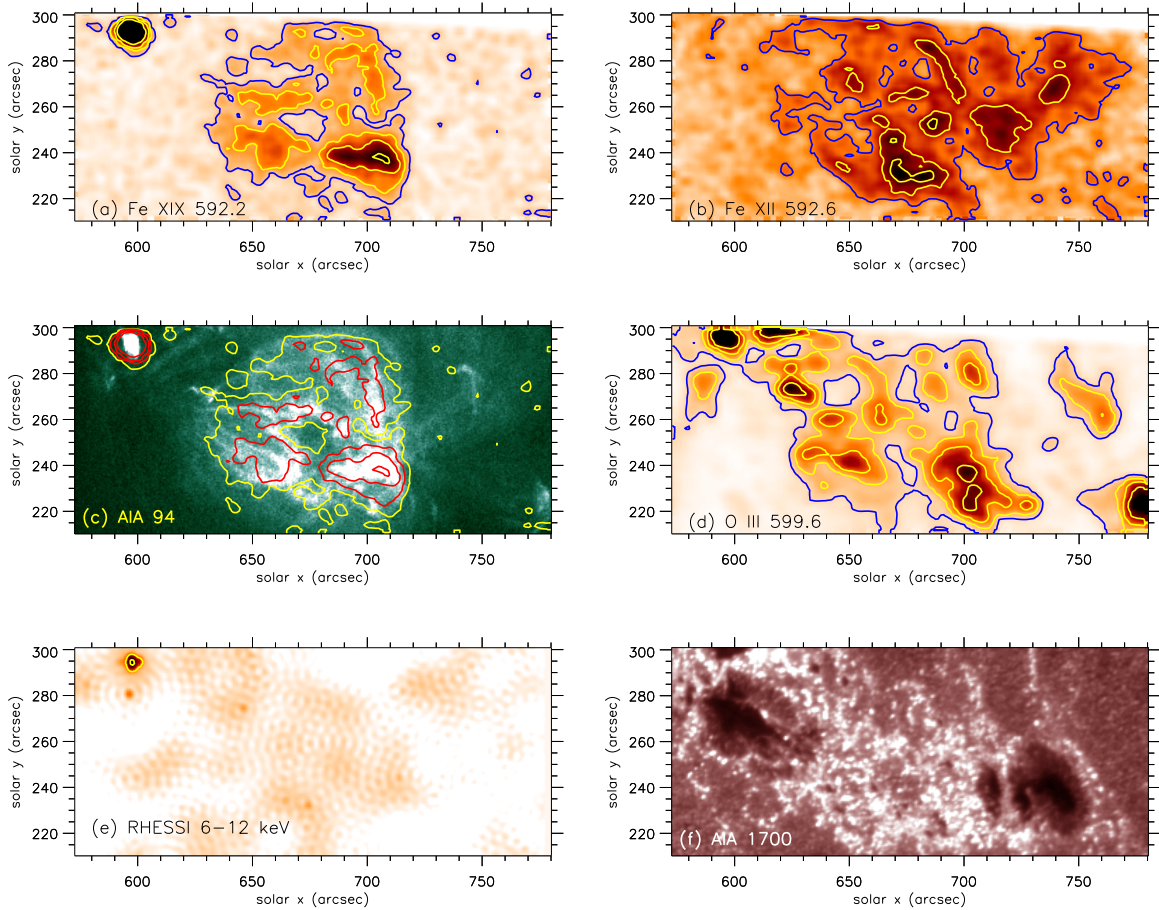
Figure 2. Images of AR 11726 obtained with EUNIS-13, AIA, and *RHESSI* between 17:32:45 and 17:33:26 UT on 2013 April 23. (a) Integrated intensity of the Fe XIX line at 592.2 Å, with contour levels of 4 (blue) and 8, 16, and 32 erg cm^{-2} s^{-1} sr^{-1} (yellow). (b) Integrated intensity of the Fe XII line at 592.6 Å, with contour levels of 8.25 (blue) and 16.5 and 24.75 (yellow). (c) AIA 94 Å image obtained closest in time (17:33:02 UT) to the central time of the EUNIS raster (17:33:06 UT), with the same Fe XIX contours shown in (a). (d) Integrated intensity of O III 599.6 Å, with contour levels of 50 (blue) and 100, 200, 400 erg cm^{-2} s^{-1} sr^{-1} (yellow). (e) *RHESSI* image at 6–12 keV, with contour levels of 0.04 and 0.12 photons cm^{-2} s^{-1} arcsec^{-2} (yellow). (f) AIA 1700 Å image obtained closest in time (17:32:55 UT) to the central time of the EUNIS raster, showing locations of sunspots.

over pixels in which the Fe XII 592.6 Å line intensity exceeds one-fourth (8.25 erg cm^{-2} s^{-1} sr^{-1}) its maximum value (33) while the Fe XIX 592.2 Å line intensity remains less than 4; we consider this to be the average active region spectrum outside the core. Figure 1(b) shows the spectrum averaged over pixels in which the Fe XII line intensity exceeds one-half (16.5) its maximum value; we consider this to be the average active region spectrum in area of bright coronal emission. Figure 1(c) shows the spectrum averaged over pixels in which the Fe XIX line intensity is between 4 and 16 erg cm^{-2} s^{-1} sr^{-1}; this is the active region's hot core. Figure 1(d) shows the spectrum averaged over pixels in which the Fe XIX intensity is between 16 and 64; this is the brightest Fe XIX emission in the active region outside the microflare, possibly remnant emission from the microflare observed by *RHESSI* near this location between 17:17:20 and 17:23:14 UT.

We coaligned the EUNIS-13 Fe XIX image of AR 11726 obtained between 17:32:45 and 17:33:26 UT with the AIA 94 Å image obtained closest to the central time of the EUNIS raster. Figure 2(c) shows the AIA 94 Å image obtained at 17:33:02 UT overplotted with the same Fe XIX contours drawn in 2a. The 75 × 32 EUNIS array of 2″.77 × 2″.82 pixels was CONGRIDded in IDL to a 346 × 151 array of 0″.6 × 0″.6 AIA pixels, and rotated 3° clockwise (pivoting about the pixel with the maximum intensity in the microflare, toward the upper left of the image).

We estimate the uncertainty in the coalignment to be ≈5″. The microflare's larger apparent size in EUNIS-13 images than in the AIA image may be due to differences between the spatial resolutions given above. The overall appearance of the 94 Å AIA image is similar to that of the Fe XIX EUNIS-13 image, but a close inspection reveals some significant differences. These will be addressed in future work. For context purposes we show in Figure 2(d) an intensity image of the O III line at 599.6 Å, formed at temperature (≈0.1 MK) characteristic of the lower transition region, and in 2f we show the AIA 1700 Å image obtained at 17:32:55 UT, which reveals the locations of sunspots.

GOES light curves show that the Sun was quiet during the EUNIS-13 flight. *GOES* lists 10 flares in AR 11726 on 2013 April 23. The last to occur before the EUNIS-13 launch (17:30 UT) was a C2.5 event that ended at 15:20 UT, and the first to occur after the EUNIS-13 flight was a C1.8 event that started at 19:29 UT. The *GOES* light curve between 16:00 and 18:00 UT shows a nearly-constant background at about a B5 level, with a few bumps and wiggles, none of which exceeds B7. *RHESSI* shows a series of six microflares in AR 11726 between about 17:05 and 17:37 UT, all of which appear in only the 3–6 and 6–12 keV channels. The first occurred 17:05:12–17:08:08 UT centered near (+580″, +280″); the second occurred 17:09:20-17:11:00 centered near (+625″, +275″); the third occurred 17:17:20–17:23:14 centered near

(+695″, +245″); the fourth 17:25:08–17:27:00 near (+595″, +295″); the fifth 17:29:24-17:31:24 near (+600″, +300″); and the sixth 17:32:38–17:37:08 near (+595″, +295″). A *RHESSI* image obtained during the EUNIS-13 flight is shown in Figure 2(e). The only significant 6–12 keV emission in this figure, averaged over the time interval covering the first full vertical EUNIS raster (17:32:45–17:33:26 UT), is in the microflare around (+595″, +295″).

4. RESULTS

Here we present our results on the extent of the faint Fe XIX emission in AR 11726, the emission measure of the faint hot plasma, and relative Doppler velocities across the active region as possible markers of chromospheric evaporation. Analyses of the microflare, of time variability observed in the region, and of the temperature response of AIA's EUV channels will be the subjects of later investigations.

4.1. Extent of Faint Fe XIX Emission

Our detection of faint hot ($\sim$10 MK) line emission in spatially resolved EUV spectra observed from a large portion of an active region's non-flaring area provides the strongest evidence to date for the nanoflare heating model of the solar corona. Figure 2(a) shows that Fe XIX emission is observed over an extensive portion of the active region. It is brightest in the microflare toward the upper left around (+595″, +295″), where the maximum intensity is 186 erg cm^{-2} s^{-1} sr^{-1}; it is weaker in the lower center around (+700″, +240″), where the maximum intensity is 35.3 (possibly remnant emission from the microflare observed by *RHESSI* from 17:17:20 to 17:23:14 UT); and much weaker everywhere else. The Fe XIX intensity exceeds 4 (the outer contour shown in Figures 2(a) and (c)) in 629 of the EUNIS 2″.77 × 2″.82 pixels, excluding the microflare in the upper left. This covers a total solar surface area of 4920 arcsec^2 (2.58×10^9 km^2), which corresponds to 64% of the area that appears bright in "standard" coronal emission (the area within the outer contour of Fe XII shown in Figure 2(b)). Similarly, the Fe XIX line intensity lies between 4 and 16 erg cm^{-2} s^{-1} sr^{-1} over a solar surface area of 4640 arcsec^2 (2.44×10^9 km^2), which corresponds to 61% of the area within the outer contour of Fe XII. Finally, the Fe XIX intensity lies between 16 and 64 over an area of 274 arcsec^2 (1.44×10^8 km^2), possibly corresponding to residual emission from the microflare observed by *RHESSI* between 17:17:20 and 17:23:14 UT.

We observe no Fe XIX emission in the spatially resolved spectra from the large tract of quiet area east of AR 11726. We averaged EUNIS spectra over 151 of the 2″.77 slit pixels that covered this quiet area during the first full northward raster scan, i.e., the same exposures used to obtain the spectra in Figure 1 and the images in Figure 2. The total area over which the quiet spectrum was averaged was 418″ × 90″. There is no emission line evident around 592.2 Å in this quiet spectrum. Thus Fe XIX emission, if present in the quiet area, is too faint to be detected by EUNIS-13. The upper limit for this emission is discussed in Section 4.2.

4.2. Emission Measure of Faint Hot Plasma

The emission measure EM is widely used to characterize the amount of emitting plasma as a function of temperature

(Pottasch 1963, 1964; Harrison & Thompson 1991; Landi & Landini 1997) in a given source. The EM is derived from observed line intensities, and depends upon various quantities (density, element abundances, ionization state, atomic physics parameters) that are not necessarily well known. It is usually assumed that any given emission line originates in plasma at and near the line's "formation temperature," i.e., the temperature at which the line's "contribution function" G (which depends upon the given element's temperature-dependent ionization fractions) is maximized. However, this assumption can break down when plasma that is heated by an impulsive burst of energy does not have time to settle into ionization equilibrium. This can happen in the case of nanoflare heating (Bradshaw & Cargill 2006; Reale & Orlando 2008), for which Bradshaw & Klimchuk (2011) find that it is far more significant at low densities (10^7–10^8 cm^{-3}) than it is at larger densities (10^9 cm^{-3}). The density of the solar atmosphere at the site of impulsive nanoflare heating is generally not known, so we cannot say whether the Fe XIX emission observed by EUNIS-13 was or was not affected by ionization non-equilibrium. Nevertheless, for purposes of providing quantities against which previous and future observations can be compared, we estimate the emission measure of the plasma that produces the Fe XIX emission that we observed under the assumption of ionization equilibrium. If the plasma is *not* in ionization equilibrium, this method will underestimate the amount of material at that line's temperature (Bradshaw & Klimchuk 2011).

With the maximum value of the contribution function $G_{\max}$ (in units of intensity per emission measure, i.e., erg cm^3 s^{-1} sr^{-1}) derived from CHIANTI v.7.1 (Dere et al. 1997, Landi et al. 2013), we estimate the emission measure EM (cm^{-5}) at the formation temperature $T_{\max}$ (the temperature at which the maximum value of the contribution function occurs) of a line whose intensity I (erg cm^{-2} s^{-1} sr^{-1}) is measured by EUNIS: EM = $I/G_{\max}$. Absent a definitive absolute radiometric calibration for EUNIS-13 we cannot yet calculate absolute values of the EM; however, because Fe XIX 592.2 Å (formed at $T \approx$ 8.9 MK) and Fe XII 592.6 Å (formed at $T \approx$ 1.6 MK) are very close in wavelength, the difference between EUNIS-13 responsivities for these two lines is negligible. Therefore, using these two lines we can estimate the ratio of the emission measures at $\approx$8.9 and $\approx$1.6 MK.

Using CHIANTI's "gofnt.pro" procedure (for which we select the CHIANTI ionization equilibrium file, the coronal element abundances of Feldman et al. 1992, and a constant density of 3×10^9 cm^{-3} typical of the active solar corona) we derive $G_{\max}$ = 9.84×10^{-27} for Fe XIX and $G_{\max}$ = 1.06×10^{-26} for Fe XII. Repeating the calculation for each line using densities of 1×10^9 and 9×10^9 cm^{-3} reveals that the contribution function for Fe XIX varies by only $\pm 0.29\%$ over this density range, while that for Fe XII varies by $\pm 32\%$. Thus, based only on uncertainties in the electron density of the emitting volume, the uncertainties on the EM ratios are 32%. E. Landi (2014, private communication) points out that the current Fe XII contribution functions are comparatively uncertain, requiring future modifications, so the actual uncertainties on the EM ratios are larger than 32%. The integrated intensity of the Fe XIX line derived from the averaged profile displayed in Figure 1(a) is 0.808 erg cm^{-2} s^{-1} sr^{-1}, from which we derive EM = 8.22×10^{25} cm^{-5}. The integrated intensity of the Fe XII line derived from the same averaged spectrum is 11.5, from which we derive EM = 1.08×10^{27} cm^{-5}. (Interestingly, these values are comparable to those derived by Patsourakos & Klimchuk 2009 for an impulsively heated

active region model.) Thus, from Figure 1(a), the Fe XIX/Fe XII EM ratio is ≈0.076. Values for the emission measure ratios corresponding to (b)–(d) of Figure 1 (0.23, 0.59, and 3.2, respectively) were similarly calculated with the Fe XIX (4.14, 5.81, and 23.9) and Fe XII (19.2, 10.6, and 8.08) intensities derived from fits to the average line profiles displayed.

Although no Fe XIX emission line is evident in the spatially averaged quiet spectrum described in Section 4.1, we applied the same "fit structure" as above to fit all four lines in the 591.0–593.5 Å waveband of the average quiet spectrum, and interpret the resulting integrated intensity (0.0082 erg cm^{-2} s^{-1} sr^{-1}) at 592.2 Å as an upper limit on Fe XIX emission. The corresponding Fe XII 592.6 Å intensity is 1.1, from which we derive an upper limit of 0.0081 on the ratio of the Fe XIX to Fe XII emission measures in the quiet area.

4.3. Relative Doppler Velocities

For Fe XIX, we used pixels in which the line's integrated intensity exceeds 10 erg cm^{-2} s^{-1} sr^{-1} (see Figure 2(a)) to obtain the reference wavelength and its associated 1σ scatter (592.171 ± 0.031 Å). All of the Fe XIX wavelengths derived from fits to the profiles in Figure 1 lie within 1σ of this reference value. We repeated the calculation for the second and third EUNIS rasters over the region, and found that the reference wavelengths differ from each other by only 2 mÅ, indicating that there is no significant instrumental wavelength shift as a function of time. The 1σ wavelength scatter corresponds to a velocity of 15.4 km s^{-1}, which we take to be the uncertainty on the Fe XIX relative Doppler velocity measurements. Relative Doppler velocity contours of ±15 and ±30 km s^{-1} are displayed in Figure 3(a), where blue corresponds to upward (negative) velocities and red to downward (positive). Velocities are displayed only for raster elements in which the integrated line intensity exceeds 4 (see Figure 2(a)). The contours in Figure 3(a) indicate that there is no significant flow pattern in this active region. For example, the microflare in the upper left is not predominantly blueshifted, and the Fe XIX emission throughout the region is not predominantly redshifted. There are only small patches throughout the region in which velocities are significant.

For Fe XII, we also used pixels in which the line's integrated intensity exceeds 10 erg cm^{-2} s^{-1} sr^{-1} (see Figure 2(b)) to obtain the reference wavelength and its associated 1σ scatter (592.619 ± 0.021 Å). None of the Fe XII wavelengths derived by fitting the profiles displayed in Figure 1 differs significantly from this reference value. We again repeated the calculation for the second and third EUNIS rasters over the region, and found that the wavelengths differ from each other by only 4 mÅ, further indicating that there is no significant instrumental wavelength shift as a function of time. The 1σ wavelength scatter corresponds to a velocity of 10.8 km s^{-1}, which we take to be the uncertainty on the Fe XII relative Doppler velocity measurements. Relative Doppler velocity contours of ±10 and ±20 km s^{-1} are displayed in Figure 3(b), where velocities are displayed only for raster elements in which the integrated line intensity exceeds 8.25 (see Figure 2(b)). Here, too, there is no significant flow pattern that might suggest that material is falling down into the active region core from elsewhere (e.g., the microflare).

5. DISCUSSION AND INTERPRETATION

We interpret the extensive, faint Fe XIX line emission observed in AR 11726 by EUNIS-13 as strong evidence for the "nanoflare
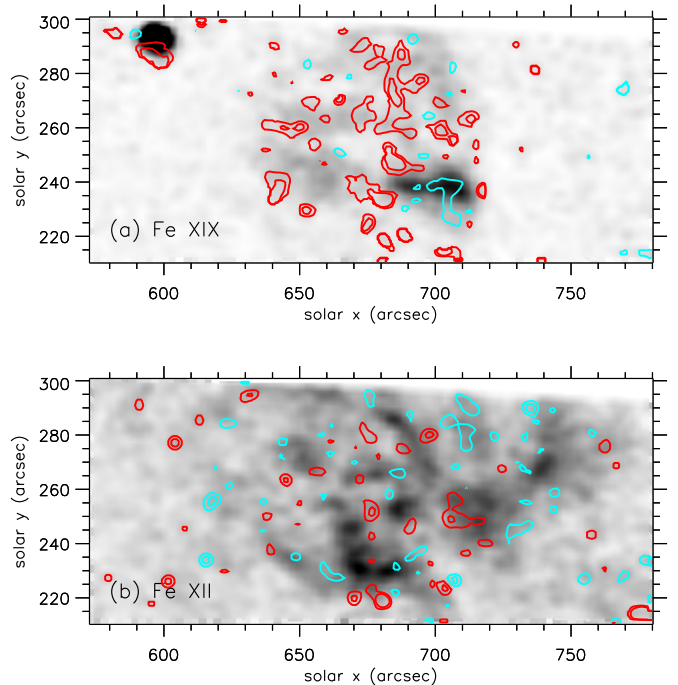

Figure 3. Relative Doppler velocity contours for (a) Fe XIX 592.2 Å and (b) Fe XII 592.6 Å, plotted over their respective integrated intensity images of AR 11726. We use black and white images to improve the visibility of the red and blue contours. Red contours represent downward (positive) velocities, and blue contours represent upward (negative) velocities. The levels are (a) ±15 and ±30 km s^{-1}, and (b) ±10 and ±20 km s^{-1}, which correspond to the 1σ scatter and twice the 1σ scatter in the reference wavelengths described in the text. This reveals no significant outpouring of heated material from the microflare around (+595″, +295″), which rules out the microflare as the source of the faint, pervasive Fe XIX emission in the active region.

heating" model of the solar corona. First, the Fe XIX emission (with intensity in excess of 4 erg cm^{-2} s^{-1} sr^{-1}, shown as the outer contour in Figure 2(a)) originates from a large area (4920 arcsec^2) within the region, which covers about 64% of the area in which the Fe XII intensity exceeds one-fourth its maximum value (the outer contour in Figure 2(b)). Second, the emission measure ratios of hot (8.9 MK) to cooler (1.6 MK) plasma are (a) ≈0.076 for areas outside the AR core (I(Fe XII) > 8.25, I(Fe XIX) < 4), and (b) ≈ 0.59 for areas inside the core. Although highly uncertain (as described above), both of these ratios indicate a smaller emission measure at flare temperatures (∼10 MK) than at ordinary coronal temperatures (1–2 MK), consistent with the nanoflare heating concept. Third, the relative Doppler velocity maps indicate no large-scale relative Doppler velocity flows throughout or across the region, which rules out the microflare around (+595″, +295″) (seen by *RHESSI* but not by *GOES*) as the source of the pervasive, faint Fe XIX emission. In other words, we find no spectroscopic evidence for chromospheric evaporative upflows in the microflare that may lead to subsequent downflows of ≈8.9 MK plasma throughout the region. This absence of a significant flow pattern supports the idea that the corona is being impulsively heated in situ by some process (magnetic reconnection, wave dissipation, or some other mechanism) during unresolved nanoflare events.

It is interesting that the Fe XII emission from the microflare is less pronounced than that of Fe XIX 592.2 Å or O III 599.6 Å; that is, the intensity of Fe XII 592.6 Å in the microflare is rather small compared with values observed elsewhere in the region. We examined the Si XI line at 580.920 Å, formed at the same

6

temperature (≈ 1.6 MK) as that of Fe XII, to see if it showed similar behavior. It does, but not quite as much as in the case of Fe XII. For Si XI, however, we note that CHIANTI v. 7.1 shows a pair of O II lines at 580.971 Å and 580.978 Å that is not only blended with the Si XI line at 580.920, but is also theoretically expected to dominate the Si XI emission. CHIANTI also shows a pair of O II lines at 580.404 Å and 580.410 Å, whose summed intensity relative to the summed intensity of the O II pair blended with Si XI is insensitive to temperature and density, i.e., I(O II 580.971 + 580.978)/I(O II 580.404 + 580.410) = 1.88 ± 0.01 for $7.0 \leqslant \log n_e \leqslant 13.0$ (at the lines' formation temperature of 0.035 MK), and 1.92 ± 0.05 for $4.0 \leqslant \log T \leqslant 6.0$ (at $\log n_e = 10.0$). Combining these ratios with the observed line intensities shows that only in the microflare does O II contribute 30–40% of the total intensity measured at 580.97 Å; elsewhere in the active region the average ratio is about 7%. Removing the O II blend from the Si XI intensity yields a relatively fainter microflare in Si XI emission. This supports our observation with Fe XII emission that the microflare really is comparatively fainter in its coronal ($T \approx 1.6$ MK) emission than it is in its transition region ($T \approx 0.1$ MK) or its hot ($T \approx 8.9$ MK) emission. We mention this here because it is relevant to the Fe XII 592.6 Å line emission, for which we have presented the first imaged solar active region.

We examined spatially resolved and spatially averaged spectra over an extensive tract of quiet area west of AR 11726, but found no evidence of Fe XIX emission in that area. Such emission will be sought during the future EUNIS flight, which will include a new spectral bandpass to observe strong emission lines of Fe XVIII (93.932 Å, the line for which the AIA 94 Å channel was designed, and 103.948 Å) and Fe XIX (108.355 and 101.550 Å). This instrument will be specifically tailored to observe the faint hot emission predicted by nanoflare heating models, and should enable us to obtain more definitive measurements in active regions than could be achieved with EUNIS-13.

6. SUMMARY AND CONCLUSIONS

We present spatially resolved, EUV spectroscopic measurements of pervasive, faint Fe XIX 592.2 Å line emission in AR 11726 observed by EUNIS-13. The Fe XIX line emission, formed at $T \approx 8.9$ MK, provides strong support for nanoflare heating models of the solar corona; it is observed over an area in excess of 4920 arcsec^2 (2.58×10^9 km^2), which covers about 64% of the area in which the Fe XII intensity exceeds one-fourth its maximum value. With its cooled detectors, high sensitivity, and high spectral resolution, EUNIS-13 resolves the lines of Fe XIX at 592.2 Å and Fe XII at 592.6 Å ($T \approx 1.6$ MK), enabling us to compare emission measures at flare temperatures with those at standard active region temperatures. Inside the active region core the average emission measure ratio is ≈ 0.59, while just outside the core it is ≈ 0.076; however, in light of uncertainties related to the status of the plasma's ionization balance as well as uncertainties in the Fe XII contribution functions, these ratios must be treated with caution. No *GOES* events occurred in the region less than two hours before the rocket flight, but a microflare was observed north and east of the region with *RHESSI* and EUNIS during the flight. The absence of large, significant upward velocities anywhere in the region, particularly in the microflare, indicates that the pervasive Fe XIX emission is not propelled outward from the microflare site, but most likely is produced by localized impulsive heating (due to reconnection events, wave dissipation, or some other mechanism) consistent with the nanoflare heating model of the solar corona.

REFERENCES

Alfvén, H. 1947, MNRAS, 107, 211
Boerner, P., Edwards, C., Lemen, J., et al. 2012, SoPh, 275, 41
Bradshaw, S. J., & Cargill, P. J. 2006, A&A, 458, 987
Bradshaw, S. J., & Klimchuk, J. A. 2011, ApJS, 194, 26
Bradshaw, S. J., Klimchuk, J. A., & Reep, J. W. 2012, ApJ, 758, 53
Brooks, D. H., Fischbacher, G. A., Fludra, A., et al. 1999, A&A, 347, 277
Brosius, J. W. 2003, ApJ, 586, 1417
Brosius, J. W., & Holman, G. D. 2009, ApJ, 692, 492
Brosius, J. W., & Holman, G. D. 2012, A&A, 540, A24
Brosius, J. W., & Phillips, K. J. H. 2004, ApJ, 613, 580
Brosius, J. W., Rabin, D. M., & Thomas, R. J. 2007, ApJL, 656, L41
Brosius, J. W., Rabin, D. M., & Thomas, R. J. 2008a, ApJ, 682, 630
Brosius, J. W., Rabin, D. M., Thomas, R. J., & Landi, E. 2008b, ApJ, 677, 781
Cargill, P. J. 1994, ApJ, 422, 381
Cargill, P. J. 2013, A&G, 54, 3.16
Cirtain, J. W., Golub, L., Winebarger, A. R., et al. 2013, Natur, 493, 501
Czaykowska, A., De Pontieu, B., Alexander, D., & Rank, G. 1999, ApJL, 521, L75
Davila, J. M. 1987, ApJ, 317, 514
de Pontieu, B., McIntosh, S. W., Carlsson, M., et al. 2011, Sci, 331, 55
de Pontieu, B., McIntosh, S. W., Hansteen, V. H., & Schrijver, C. J. 2009, ApJL, 701, L1
Del Zanna, G., & Mason, H. E. 2005, A&AS, 433, 731
Dere, K. P., Landi, E., Mason, H. E., Monsignori-Fossi, B. C., & Young, P. R. 1997, A&AS, 125, 149
Edlén, B. 1943, ZA, 22, 30
Feldman, U., Behring, W. E., Curdt, W., et al. 1997, ApJS, 113, 195
Feldman, U., Mandelbaum, P., Seely, J. L., Doschek, G. A., & Gursky, H. 1992, ApJS, 81, 387
Glencross, W. M. 1975, ApJL, 199, L53
Grotrian, W. 1939, NW, 27, 214
Harrison, R. A., & Thompson, A. M. (eds.) 1991, Intensity Integral Inversion Techniques: A Study in Preparation for the SOHO Mission, RAL-91-092, RAL Technical Report
Haugan, S. V. H. 1997, CDS Software Note No. 47, http://solar.bnsc.rl.ac.uk/swnotes/cds_swnote_47.pdf
Hollweg, J. V. 1984, ApJ, 277, 392
Ionson, J. A. 1978, ApJ, 226, 650
Jess, D. B., Rabin, D. M., Thomas, R. J., et al. 2008, ApJ, 682, 1363
Judge, P. G., de Pontieu, B., McIntosh, S. W., & Olluri, K. 2012, ApJ, 746, 158
Klimchuk, J. A. 2009, in ASP Conf. Ser. 415, The Second Hinode Science Meeting: Beyond Discovery–Toward Understanding, ed. B. Lites, M. Cheung, T. Magara, J. Mariska, & K. Reeves (San Francisco, CA: ASP), 221
Klimchuk, J. A., Patsourakos, S., & Cargill, P. J. 2008, ApJ, 682, 1351
Ko, Y.-K., Doschek, G. A., Warren, H. P., & Young, P. R. 2009, ApJ, 697, 1956
Lin, R. P., Schwartz, R. A., Kane, S. R., Pelling, R. M., & Hurley, K. C. 1984, ApJ, 283, 421
Landi, E., & Landini, M. 1997, A&A, 327, 1230
Landi, E., Young, P. R., Dere, K. P., Del Zanna, G., & Mason, H. E. 2013, ApJ, 763, 86
Lemen, J. R., Title, A. M., Akin, D. J., et al. 2012, SoPh, 275, 17
McIntosh, S. W., de Pontieu, B., Carlsson, M., et al. 2011, Nature, 475, 477
Milligan, R. O., Gallagher, P. T., Mathioudakis, M., et al. 2006, ApJL, 638, L117
Mulu-Moore, F. M., Winebarger, A. R., & Warren, H. P. 2011, ApJL, 724, L6
Parker, E. N. 1983, ApJ, 264, 642
Parker, E. N. 1988, ApJ, 330, 474
Patsourakos, S., & Klimchuk, J. A. 2009, ApJ, 696, 760
Pottasch, S. R. 1963, ApJ, 137, 945
Pottasch, S. R. 1964, SSRv, 3, 816
Reale, F., McTiernan, J., & Testa, P. 2009a, ApJL, 704, L58
Reale, F., & Orlando, S. 2008, ApJ, 684, 715
Reale, F., Testa, P., Klimchuk, J. A., & Parenti, S. 2009b, ApJ, 698, 756
Reep, J. W., Bradshaw, S. J., & Klimchuk, J. A. 2013, ApJ, 764, 193
Schmelz, J. T., Kashyap, V. L., Saar, S. H., et al. 2009a, ApJ, 704, 863

Schmelz, J. T., Saar, S. H., DeLuca, E. E., et al. 2009b, ApJL, 693, L131
Sylwester, B., Sylwester, J., & Phillips, K. J. H. 2010, A&A, 514, A82
Teriaca, L., Falchi, A., Falciani, R., Cauzzi, G., & Maltagliati, L. 2006, A&A, 455, 1123
Testa, P., De Pontieu, B., Martnez-Sykora, J., et al. 2013, ApJL, 770, L1
Testa, P., & Reale, F. 2012, ApJL, 750, L10
Testa, P., Reale, F., Landi, E., DeLuca, E. E., & Kashyap, V. 2011, ApJ, 728, 30
van Ballegooijen, A. A., Asgari-Targhi, M., Cranmer, S. R., & DeLuca, E. E. 2011, ApJ, 736, 3
Viall, N. M., & Klimchuk, J. A. 2011, ApJ, 738, 24

Viall, N. M., & Klimchuk, J. A. 2012, ApJ, 753, 35
Viall, N. M., & Klimchuk, J. A. 2013, ApJ, 771, 115
Wang, T. J., Brosius, J. W., Thomas, R. J., Rabin, D. M., & Davila, J. M. 2010, ApJS, 186, 222
Wang, T. J., Thomas, R. J., Brosius, J. W., et al. 2011, ApJS, 197, 32
Warren, H. P., Brooks, D. H., & Winebarger, A. R. 2011, ApJ, 734, 90
Winebarger, A. R., Walsh, R. W., Moore, R., et al. 2013, ApJ, 771, 21
Winebarger, A. R., Warren, H. P., Schmelz, J. T., et al. 2012, ApJL, 746, L17